Journal of Neurochemistry

WILEY

Journal of Neurochemistry JNC The Official Journal of the International Society for Neurochemistry

ORIGINAL ARTICLE OPEN ACCESS

Autism Spectrum Disorder

Regulation of Dendrite and Dendritic Spine Formation by TCF20

Ersilia Vinci[1] | Stefania Beretta[1] | Veronica Colombo[1] | Antonio Zippo[1] | Alberto Catanese[2,3] | Christoph Wiegreffe[4] | Stefan Britsch[4] | Tobias Boeckers[2,3] | Chiara Verpelli[1] | Carlo Sala[1]

[1]CNR Neuroscience Institute, Milano, Vedano al Lambro, Italy | [2]Institute of Anatomy and Cell Biology, University of Ulm, Ulm, Germany | [3]German Center for Neurodegenerative Diseases (DZNE), Ulm, Germany | [4]Institute of Molecular and Cellular Anatomy, University of Ulm, Ulm, Germany

Correspondence: Carlo Sala (carlo.sala@in.cnr.it)

Received: 7 June 2024 | **Revised:** 24 October 2024 | **Accepted:** 11 December 2024

Funding: This work was supported by Fondation Jerome Lejeune (project # 2054-SC2021A to C.S. and project #1938 to C.V.), the Comitato Telethon Fondazione Onlus (grant no. GMR22T1061 to C.S.) and Else Kröner Foundation to T.B.

Keywords: BDNF | dendritic spines | nruodevelopmental disease | synapses

ABSTRACT

Mutations in the Transcription Factor 20 (TCF20) have been identified in patients with autism spectrum disorders (ASDs), intellectual disabilities (IDs), and other neurological issues. Recently, a new syndrome called TCF20-associated neurodevelopmental disorders (TAND) has been described, with specific clinical features. While TCF20's role in the neurogenesis of mouse embryos has been reported, little is known about its molecular function in neurons. In this study, we demonstrate that TCF20 is expressed in all analyzed brain regions in mice, and its expression increases during brain development but decreases in muscle tissue. Our findings suggest that TCF20 plays a central role in dendritic arborization and dendritic spine formation processes. RNA sequencing analysis revealed a downregulation of pre- and postsynaptic pathways in TCF20 knockdown neurons. We also found decreased levels of GABRA1, BDNF, PSD-95, and c-Fos in total homogenates and in synaptosomal preparations of knockdown TCF20 rat cortical cultures. Furthermore, synaptosomal preparations of knockdown TCF20 rat cortical cultures showed significant downregulation of GluN2B and GABRA5, while GluA2 was significantly upregulated. Overall, our data suggest that TCF20 plays an essential role in neuronal development and function by modulating the expression of proteins involved in dendrite and synapse formation and function.

1 | Introduction

Among the several gene mutations identified as high-risk factors for the pathogenesis of neurodevelopmental disorders, de novo mutations of TCF20 (Transcription Factor 20) have been identified in large-scale exome sequencing data of patients with intellectual disability and autism. TCF20 encodes a transcriptional co-regulator (Darvekar et al. 2012) that was initially identified by its ability to bind the stromelysin-1 PDGF-responsive element (SPRE), an element of the stromelysin-1 (matrix metalloproteinase-3/MMP3) promoter (Sanz, Moscat, and Diaz-Meco 1995). TCF20 (also termed AR1, SPBP, SPRE-binding protein) is localized to the nucleus and has been found to play a role as a transcriptional co-activator in modulating the transcriptional activity

Abbreviations: ASD, autism spectrum disorders; BDNF, brain derived neurotrophic factor; Dlg4, discs large MAGUK scaffold protein 4; GABRA1, gamma-aminobutyric acid type A receptor subunit alpha1; GABRA5, gamma-aminobutyric acid type A receptor subunit alpha5; GAD65, glutamic acid decarboxylase 65-kilodalton isoform; GDB, gelatin detergent buffer; GFP, green fluorescent protein; GluA2, α-amino-3-hydroxy-5-methyl-4-isoxazolepropionic acid receptor subunit 2A; GluN2B, N-methyl D-aspartate receptor subtype 2B; IDs, intellectual disabilities; MMP3, matrix metalloproteinase-3; PDGF, platelet-derived growth factor; PMS, Phelan-McDermid syndrome; PSD-95, postsynaptic density protein 95; RRID, research resource identifier; SCR, scramble; shRNAs, short hairpin RNAs; SPRE, PDGF-responsive element; SPRE, stromelysin-1 PDGF-responsive element; TAND, TCF20-associated neurodevelopmental disorders; TCF20, transcription factor 20.

of Sp1, c-Jun, Est1, Pax6 (Gburcik et al. 2005; Rekdal, Sjøttem, and Johansen 2000) and RNF4 (Darvekar et al. 2012; Rekdal, Sjøttem, and Johansen 2000; Sjøttem et al. 2007; Lyngsø et al. 2000). TCF20 is highly expressed in several brain areas (Gray et al. 2004), that are involved in high cognitive functions, including the cortex, hippocampus, and cerebellum (Lein et al. 2007).

An increasing number of patients with TCF20 mutations, including de novo and inherited variants, have been recently reported (Babbs et al. 2014; Lelieveld et al. 2016; Schäfgen et al. 2016; Study 2017; Bowling et al. 2017). For these patients, the described clinical features include mild-to-moderate ID with or without ASD and accompanying features such as proportionate overgrowth and muscular hypotonia (Babbs et al. 2014; Lelieveld et al. 2016; Schäfgen et al. 2016; Study 2017).

Recently, two papers were published providing more clinically relevant information for clinicians, researchers, and families of affected individuals. These papers characterized several variants in TCF20 that were unique to different families (Torti et al. 2019; Vetrini et al. 2019). Both neurologic and non-neurologic features were described in detail, strongly supporting a major role for TCF20 mutations/deletions in causing IDs and ASDs (Torti et al. 2019; Babbs et al. 2014; Schäfgen et al. 2016; Smeland et al. 2017; Vetrini et al. 2019). Thus, mutations in TCF20 associated with ataxia, hypotonia, autistic behaviors, and sleep disturbances have been classified as causing TAND (TCF20-associated neurodevelopmental disorders) (Torti et al. 2019; Vetrini et al. 2019; Babbs et al. 2014).

Interestingly, TCF20 is located in chromosome 22q13.2 region, which is a region also deleted in Phelan-McDermid syndrome (PMS), where several other genes are deleted, including the major candidate gene SHANK3 (Sala et al. 2015; Vicidomini et al. 2017; Mossa et al. 2021; Upadia et al. 2018). Like TAND syndrome, PMS involves a range of phenotypes including global developmental delay, intellectual disability, neonatal hypotonia, autism, and autistic-like behaviors. PMS is considered a syndromic form of ASD (Phelan 2008; Phelan and McDermid 2012; Kurtas et al. 2018). TCF20 mutations or microdeletions have also been found in patients with PMS, suggesting a causative role for TCF20 deletions/mutations in neurological dysfunction in these patients (Upadia et al. 2018; Kurtas et al. 2018; Torti et al. 2019).

However, the role of TCF20 in brain development and function remains to be clarified. Recent reports suggest that TCF20 promotes the neurogenesis of mouse embryos, but little is known about its molecular function in neurons. Here, we provide evidence that TCF20 is an essential player in neuronal development and function by regulating dendrite and synapse formation and function.

2 | Materials and Methods

2.1 | Animals

To prepare primary neuronal rat cortical cultures, pregnant female Sprague Dawley rats (*Rattus norvegicus*, RRID:MGI:5651135) were purchased from Charles River (Charles River Laboratories, Calco, Italy). C57BL/6 (RRID:MGI:2159769) wild-type mice were purchased from Charles River. Adult mice (with a weight of about 25 g) and rats (with a weight of about 120 g) were housed under constant temperature (22°C ± 1°C) and humidity (50%) conditions with a 12-h light/dark cycle and were provided with food and water ad libitum in standard cages (355 cm/square) in enriched environments (three animals for each cage). All experiments involving animals followed protocols in accordance with the guidelines established by the European Communities Council and the Italian Ministry of Health (Rome, Italy) for the correct use of laboratory animals in research (Aut. N. 582/2016-PR, 2D464.0).

2.2 | Constructs and Virus Generation

For RNA interference, four siRNA sequences targeting Tcf20 mRNA were designed using GenScript siRNA Target Finder instructions (GenScript). The following nucleotide sequences were used:

shRNA1 TGGCTAGCGAGACCTCTGG,

shRNA2 ATCTCAAGCTAGTTTCAAC,

shRNA3 GCCCAGTCCTAATTCTCAT,

shRNA4 GGCTGCTCCTTCCGATACC.

The generated short hairpin RNAs (shRNAs) were cloned into the pLVTHM-GFP (RRID:Addgene_12247) vector (Wiznerowicz and Trono 2003) using EcoRI and ClaI restriction sites. After choosing shRNA3 as best construct for interference of TCF20 (named shTCF20), we generated a scrambled sequence form of shRNA3 that was cloned into pLVTHM-GFP to obtain the control shRNA (indicated as SCR). The sequence of shRNA3 is identical to the human (Sequence ID: KF851355) and rat (Sequence ID: NM_001130574.1) TCF20 sequences. It contains only a single mismatch, located in the middle of the sequence, for the mouse TCF20 sequence (Sequence ID: XM_011245552.4). Despite this minor mismatch, shRNA3 effectively knocked down TCF20 expression in both rat and mouse cortical neurons (see Figure 5, additional data not shown).

Previously described p-Sport1-SPBP vector, encoding full-length human TCF20 (Sjøttem et al. 2007), was used to generate a construct resistant to interference by shTCF20. Site directed mutagenesis was performed using QuikChange Lightning Site-Directed Mutagenesis Kit (Agilent Technologies, cat. n. 210518/210519). In this construct, six nucleotides (C1278A, T1281C, T1284C, T1287C, T1290 C, T1293C) of the shTCF20 target site were altered, without changing the amino acid sequence of the resultant protein.

For the overexpression experiments in HEK293T cells and rat cortical neuron cultures, TCF20 sequence was subcloned from p-Sport1-SPBP vector into AscI and EcoRI sites of GW1-CMV vector, containing a GFP-tag fused at N-terminal of TCF20. GFP-318-TCF20 construct, encoding TCF20 truncated

at AA318, was made by inserting a PCR product generated from p-Sport1-SPBP using primers (5′-TAAGCAGGCGCGC CTATGCAGTCCTTTCGGGAG-3′ and 5′-TGCTTAGGAAT TCTCACCCCCGCTCCGACTG-3′) into the AscI and EcoRI sites of GW1-CMV vector, containing a GFP-tag fused at N-terminal of truncated TCF20. GFP-1079-TCF20 construct, encoding TCF20 truncated at AA1079, was made by inserting a PCR product generated from p-Sport1-SPBP using primers (5′-TAAGCAGGCGCGCCTATGCAGTCCTTTCGGGAG-3′ and 5′-TGCTTAGAATTCAAACCTGCGTTA-3′) into the AscI and EcoRI sites of GW1-CMV vector, containing a GFP-tag fused at N-terminal of truncated TCF20. GFP-1906-TCF20 construct, encoding TCF20 truncated at AA1906, was made by inserting a PCR product generated from p-Sport1-SPBP using primers (5′-TAAGCAGAATTCTCAGCTGCATTA-3′ and 5′-TGCTTA GAATTCTCAGAAGGAGCAGC-3′) into the AscI and EcoR1 sites of GFP-3237-TCF20 construct.

For viral transduction, genetically modified lentiviruses shTCF20 and SCR were produced as previously described (Lois et al. 2002; Naldini et al. 1996), and the production was carried out with 2nd and 3rd generation lentiviral transfer vectors.

2.3 | HEK293T Cell Culture

HEK293T cells (purchased by ATCC cat. CRL-3216, RRID:CVCL_0045, number of maximum passage 50, were not authenticated) were cultured at 37°C and 5% CO_2 atmosphere in DMEM (ThermoFisher) supplemented with fetal bovine serum (10%, ThermoFisher), L-Glutamine (2 mM, Euroclone), PenStrep (1%, ThermoFisher). The HEK293T cell line is not listed as a commonly misidentified cell line by the International Cell Line Authentication Committee (ICLAC; http://iclac.org/databases/cross-contaminations/). HEK293T cells were transfected using Polyethylenimine (PEI 25K) (23966-1, Polysciences) and collected 48 h after transfection.

2.4 | Primary Neuronal Cell Culture

Rat cortical neuronal cultures were prepared from embryonic day 18 (E18) embryos (Charles River) as previously described (Verpelli et al. 2010). Pregnant rats and embryos (E18) were killed by CO_2 inhalation and decapitation. A total number of 21 dams and 210 embryos were used. Isolated neurons, obtained by pulling embryos brains obtained for each dam, were plated at 250 cells/mm^2 density on 6-well plates (Euroclone) and at 75 cells/mm^2 density on cover slips in 12-well plates (Euroclone) coated with 0.01 mg/mL poly-L-lysine (Sigma-Aldrich). Neurons were cultured in Neurobasal (ThermoFisher) supplemented with the previously described B27 (Chen et al. 2008). Cells were cultured on 6-well plates for protein biochemical analysis, whereas 12-well plates with acid-treated coverslips (VWR) were used for immunocytochemical analysis. At day-in vitro 7 (DIV7), neurons were transfected using Lipofectamine 2000 (ThermoFisher). At DIV4, neurons were transduced with lentiviral vectors. Biochemical and morphological experiments were performed at DIV14.

2.5 | RNA Sequencing

Following transduction at DIV4 with shTCF20 or SCR lentiviruses, total RNA was extracted from rat cortical neuronal cultures using Trizol reagent (cat.n. 93289, Sigma) following the manufacture's instruction. Preparation of RNA library and transcriptome sequencing was conducted by Cambridge Sequencing Center (UK) of Novogene. RNA degradation and contamination were monitored on 1% agarose gels, RNA purity was checked using the NanoPhotometer spectrophotometer (IMPLEN, CA, USA), and RNA integrity and quantitation were assessed using the RNA Nano 6000 Assay Kit of the Bioanalyzer 2100 system (Agilent Technologies, CA, USA).

A total amount of 1 μg RNA per sample was used as input material for the RNA sample preparations. Sequencing libraries were generated using NEBNext Ultra TM RNA Library Prep Kit for Illumina (NEB, USA) following manufacturer's recommendations and index codes were added to attribute sequences to each sample. The clustering of the index-coded samples was performed on a cBot Cluster Generation System using PE Cluster Kit cBot-HS (Illumina) according to the manufacturer's instructions. After cluster generation, the library preparations were sequenced on an Illumina platform and paired-end reads were generated.

2.6 | Biochemical Analysis

We used rat cortical neuronal cultures prepared from E18 embryos and plated on 6-well plates. We generally obtain 6–9 6-well plates from each pregnant rat, and total homogenate or synaptosome were obtained by mixing the lysates of 2–3 6-plates. Thus, for each cortical neuronal cultures preparation we were able to obtain 3–4 independent samples that we used for the western blot (WB) analysis. Each sample was used for at least 4–6 WB for different proteins.

Mouse brains and muscle or cultured cortical neurons were lysed in pre-chilled buffered sucrose [0.32 M sucrose (Sigma-Aldrich)/4 mM HEPES-NaOH buffer (Sigma-Aldrich), pH 7.3, protease inhibitors (Sigma-Aldrich), phosphatase inhibitors (Roche)].

Samples were centrifuged at 800 *g* for 5 min at 4°C. In other cases, fractionation took place to obtain a synaptosome-enriched fraction (P2), as previously published (Vicidomini et al. 2017). Resulting samples were quantified by BCA protein assay (EuroClone) to assess protein concentration and then solubilized in 4× loading buffer [250 mM Tris, 40% glycerol, 0.008% bromophenol blue (all Sigma-Aldrich)]. All samples were boiled at 65°C for 10 min and then equal amounts (50 μg) of each sample were separated using SDS-PAGE (percentage of SDS gels from 6% to 12%, depending on the MW of the analyzed protein) and subsequently blotted on nitrocellulose membranes using the Trans-Blot Turbo System (Bio-Rad). Membranes were washed in Tris-buffered saline-Tween (TBS-T) [20 mM Tris pH 7.4, 150 mM NaCl (both Sigma-Aldrich), and 0.1% Tween 20 (Bio-Rad)]. Membranes were then incubated for at least 1 h at room temperature with 5%

milk in TBS-T to prevent non-specific binding of detection antibodies. Membranes were then incubated overnight at 4°C with primary antibody in blocking buffer (TBS-T containing 5% milk). The membranes were washed three times with TBS-T and then incubated with secondary antibodies in TBS-T and 5% milk for 1 h at room temperature. After three washes (10 min each), signal was acquired using Odissey CLx infrared imaging system (LI-COR Biosciences), and densitometry was performed using Image Studio Lite 5.2 Software (LI-COR Biosciences) and normalized against the values of the respective signal for actin.

2.7 | In Utero Electroporation

In utero electroporation experiments were carried out in compliance with the German Animal Welfare Act and approved by the respective government offices in Tübingen, Germany (TV-Nr. 1471). Electroporation of expression plasmids for SCR, shTCF20, and shTCF20 + Resistant was carried out on E14.5 C57BL/6J mice essentially as described (Wiegreffe et al. 2015, 2017). Electroporation was performed in the morning between 8.30 and 11 a.m. At least 30 min before surgery, animals were injected s.c. with carprofen solution (5 mg/kg) for analgesia. Anesthesia was induced with 5% isoflurane and maintained with 2% isoflurane delivered with 100% oxygen. After laparotomy, the uterine horns were exposed and 1 to 2 μL plasmid solution (1 μg/μL) supplemented with 0.01% FastGreen was injected with a pulled glass capillary into the lateral ventricle of each embryo. Electroporation was carried out using a CUY 21 EDIT square wave electroporator (Nepa Gene) and 5 mm electrodes, delivering five pulses of 40 V and 50 ms duration with 950 ms pauses. The uterus was then repositioned, and the abdomen sewed up. Animals were closely observed during the following days, and analgetic treatment continued for at least 2 days by injection s.c. of carprofen solution every 12 h (5 mg/kg). A total of 12 dams (weight 26–32 g, 1 dam/cage) were used in two consecutive experiments for the three experimental groups (SCR: 4, shTCF20: 4, shTCF20 + Resistant: 4). A total of 101 embryos were electroporated and 50 embryos survived. Pups were killed at postnatal day P30 by CO_2 inhalation and decapitation. The pups' brains were removed and immersion-fixed in 4% formaldehyde, 10% sucrose in phosphate-buffered saline (PBS) at 4°C overnight, washed three times in PBS and preserved in PBS containing 0.01% sodium azide. Brains were subsequently cut into 50 to 100 μm frontal sections with a vibratome (Microm HM650 V, ThermoFisher Scientific).

2.8 | Multielectrode Array (MEA) Measurements

A MaxTwo Multiwell MEA system (MaxWell Biosystems) was used to register the neuronal activity of rat cortical neuronal cultures transduced at DIV4 with shTCF20 or SCR lentiviruses.

Prior to plating, MaxWell MaxTwo 6-well plates (MaxWell Biosystems) were treated with 1% solution of sterile-filtered Tergazyme (Alconox, 1304-1) at 37°C overnight in order to increase the hydrophilicity of the surface. After removal of Tergazyme solution and disinfection with 70% ethanol for 15–20 min, the plates were washed with $PBS^{-/-}$ (Thermo Fisher Scientific) before coating the electrode area with 0.01 mg/mL poly-L-Lysine (Sigma-Aldrich) for 2 h at 37°C. Afterward, the coating solution was removed, and 100 000 cells were seeded in each well on the electrode areas. Two hours after plating, 1 mL of Neurobasal (Thermofisher) was added to each well. Presented longitudinal data originate from a minimum of three independent differentiations per cell line. Electrophysiological parameters were obtained using a system's gain of 512× with a high-pass filter from 300 Hz and a spike threshold of 5.00. During recordings, the device was kept closed and with an internal temperature of 37°C. First, the activity of the wells was monitored with a full-sensor "Activity Scan" assay in MaxLab Live software with a recording time of 20 s per electrode. Those wells displaying less than 2.5% active electrodes were not considered for further analysis (Sommer et al. 2022). Afterwards, "Network Scan" assays (in MaxLab Live software) were performed by recording only the most active subset of electrodes per well (as evaluated by a built-in algorithm in MaxLab Live software, based on the firing rate) over a period of 300 s. In order to allow a paired comparison based on the silencing of TCF20, the average value of each parameter was calculated based on all the wells belonging to the corresponding condition (shTCF20 or SCR) in each independent replicate (4 neuronal cultures).

2.9 | Immunocytochemistry

Cells were fixed in 4% paraformaldehyde, 4% sucrose in PBS [136.8 mM NaCl, 2.68 mM KCl, 10.1 mM Na_2HPO_4, and 1.76 mM KH_2PO_4, pH 7.4 (all Sigma-Aldrich)] at room temperature for 10 min. Primary antibodies were diluted in homemade gelatin detergent buffer (GDB) [30 mM phosphate buffer, pH 7.4, 0.2% gelatin, 0.5% Triton X-100, 0.8 M NaCl (all Sigma-Aldrich)] and applied o/n at 4°C. Secondary antibodies conjugate with fluorophores (Jackson ImmunoResearch Laboratories) were also diluted in GDB buffer (Verpelli et al. 2011) and applied for 1 h. DAPI staining (ThermoFisher) was carried out at a final concentration of 0.5 μg/mL. Coverslips were mounted on pre-cleaned microscope slides using Mowiol mounting medium (Osborn and Weber 1982).

2.10 | Image Acquisition and Processing

Confocal images were obtained using LSM 800 confocal microscope (Carl Zeiss) with Zeiss 20× or 63× objectives at a resolution of 1024 × 1024 pixels. Images represent averaged intensity Z-series projections of 2–7 individual images taken at depth intervals of around 0.45 μm.

Secondary and tertiary dendrites with comparable length and width were selected for dendritic spine analyses. Dendritic spine analysis was performed as described in Verpelli et al. (2011), but using Fiji/ImageJ software (US National Institutes of Health) for the quantification.

For neuronal arborization analysis, Sholl analysis was performed using Fiji/ImageJ software. Branching points intersections were counted and plotted against distance from the soma.

2.11 | Antibodies

The following primary antibodies were used for western blot: rabbit anti-β-Actin (A206, 1:1000, Sigma, RRID:AB_476693), rabbit anti-BDNF (PA5-85730, 1:500, Invitrogen, RRID:AB_2792869), rabbit anti-c-Fos (9F6, 1:250, Cell Signaling, RRID:AB_2247211), mouse anti-GABRA1 (75-136, 1:1000 NeuroMab, RRID:AB_2877288), mouse anti-GABRA5 (N415/24, 1:500, NeuroMab, RRID:AB_2877618), mouse anti-GAD65 (D5G2/5843S, 1:1000, Cell Signaling, RRID:AB_10835855), mouse anti-GluA2 (75-002, 1:400, NeuroMab, RRID:AB_2232661), mouse anti-GluN2B (75-097, 1:400, Neuromab, RRID:AB_10673405), rabbit anti-PSD-95 (D27E11, 1:1000, Cell Signaling, RRID:AB_2943447), rabbit anti-TCF20 (1:500 kindly provided by Dr. Sjøttem and published in Rekdal, Sjøttem, and Johansen 2000).

The following secondary antibodies were used for western blot: IRDye 800CW Goat anti-Rabbit (1:15000, LI-COR Biosciences, RRID:AB_10518129) and IRDye 680RD Goat anti-Mouse (1:15000, LI-COR Biosciences, RRID:AB_2895657). The following antibodies were used for immunocytochemistry: primary antibody rabbit anti-TCF20 (PA5-57816, 1:100, Invitrogen, RRID:AB_2648315), secondary antibody anti-rabbit CY3 (1:200, Jackson ImmunoResearch, RRID:AB_2337127).

2.12 | Experimental Design and Statistical Analysis

A sample size calculation was performed using GPower 3.1.9.4. Based on previous studies (Montani et al. 2017), an effect size of $d = 0.5$ was used to detect a difference between two independent means. The power was set to 80% ($1-\beta = 0.80$), with an alpha level of 0.05. No test for outliers was conducted.

For all graphic data, *n* represents the number of biological replicates, with the *n* values reported in the figure legends. Data are expressed as Mean ± Standard Error of the Mean (SEM) or as percentages. These data were analyzed for statistical significance and visualized using Prism 9 software (GraphPad, San Diego, CA). To assess the normality of the experimental data, the Shapiro–Wilk test or D'Agostino–Pearson test was applied. Depending on the normality and the number of comparisons, appropriate statistical tests were selected, as detailed in the figure legends. For comparisons between two groups, either an unpaired two-tailed *t*-test (for normally distributed data) or a Mann–Whitney test (for non-normal data) was used. When comparing more than two groups, a one-way ANOVA followed by Tukey's multiple comparisons test was performed. For experiments involving two independent variables, two-way ANOVA followed by Bonferroni correction was conducted. The significance level was set at $p \leq 0.05$.

3 | Results

3.1 | TCF20 is Differentially Expressed in Brain and Muscle During Post-Natal Mouse Development

Considering that TCF20 mutations lead to developmental disorders, IDs, and ASDs (Torti et al. 2019; Vetrini et al. 2019), we studied its expression during mouse brain development at 0, 14, 35, and 70 post-natal days (PND). The Western blot (WB) analyses of total lysates obtained from wild-type mouse brains showed that TCF20 expression is significantly increased from PND0 to PND70, suggesting its possible functional importance during the after-birth neuronal development (Figure 1A). Indeed, the increased postnatal expression of TCF20 is similar to the expression profile of PSD-95, a postsynaptic protein important in regulating synapse formation and function (Figure 1A).

To investigate the role of TCF20 in neurons, we then analyzed the area-specific protein expression in different mouse brain areas. TCF20 expression was previously investigated in the cerebral cortex of mouse embryos, where it is ubiquitously expressed (Feng et al. 2020). We performed WB analyses of total lysates of cerebral cortex, cerebellum, striatum, and hippocampus dissected from PND60 mice. Our results showed that TCF20 is ubiquitously expressed in all the considered areas without significant differences between these areas and between male and female mice (Figure 1B).

Given that patients with TAND syndromes present hypotonia (Schäfgen et al. 2016; Torti et al. 2019; Vetrini et al. 2019), we investigated TCF20 expression during mouse gastrocnemius postnatal development. The WB analyses of total gastrocnemius lysates from mice at PND 0, 14, 35, and 70 showed, in contrast to what was found in the brain, that TCF20 expression is significantly decreased during post-natal development (Figure 1C).

3.2 | Lower Dendritic Arborization and Dendritic Spine Density In Vitro and In Vivo Induced by TCF20 Knockdown in Neurons

To evaluate the function of TCF20 in neuronal and synapse morphogenesis, we designed and tested four different TCF20-specific shRNAs: shRNA1, shRNA2, shRNA3, and shRNA4. In order to choose the shRNA that strongly reduces TCF20 expression, HEK293T cells were transfected with shRNA constructs and a control scrambled shRNA (SCR). We found that all shRNAs significantly reduced TCF20 expression levels, with higher efficiency for shRNA3, which was finally chosen for our studies and referred to as shTCF20 (Figure S1A). To confirm the specificity of shTCF20 silencing activity, shTCF20 was expressed together with a construct resistant to RNA interference, referred to as Resistant, which was able to restore the expression of TCF20 protein when co-transfected with shTCF20 in HEK293T cells (Figure S1B). The shRNA3 sequence effectively knocked down TCF20 expression in both rat and mouse cortical neurons (see Figure 5, additional data not shown).

Considering that ASDs are often associated with alterations in neuronal morphology (Montani et al. 2017; Dang et al. 2018), we first investigated the effect of TCF20 silencing on dendritic branching complexity in rat cortical neuronal cultures. Neurons were transfected at 7 days in vitro (DIV7) with shTCF20 or shSCR constructs and were fixed at DIV14. Dendrite morphology of transfected neurons was then evaluated by Sholl analysis at DIV14. Branching analyses, performed on images acquired

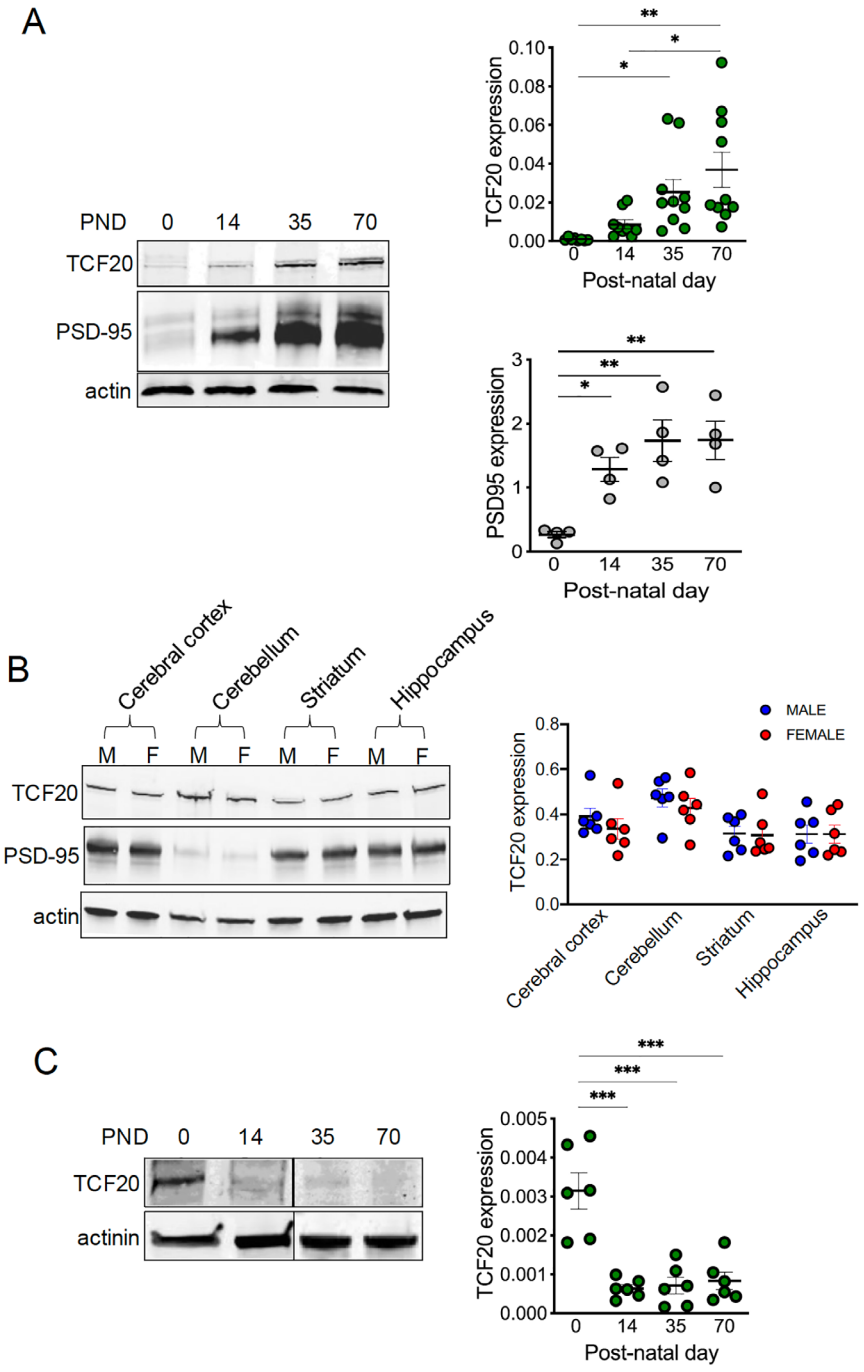

FIGURE 1 | TCF20 and PSD-95 levels increase during post-natal brain development. (A) Representative Western blot and relative quantification of TCF20 and PSD95 expression in total brain lysates derived from wild-type mice at 0, 14, 35, and 70 post-natal days. Data (fluorescent arbitrary units) are expressed as the mean ± SEM, $n = 10$ animals for all conditions; one-way ANOVA test followed by Tukey's multiple comparisons test; $^{*}p < 0.05$; $^{**}p < 0.01$, degrees of freedom between groups: 3, degrees of freedom within groups: 12; F-value: 8.39; p-value: 0.0028. $p < 0.01$; degrees of freedom between groups: 3; degrees of freedom within groups: 12; F-value: 8.39; p-value: 0.0028. (B) TCF20 is ubiquitously distributed in different brain areas of adult (PND60) wild-type mice. Western blot of total lysates in cerebral cortex, cerebellum, striatum, and hippocampus of adult male (M) and female (F) mice. Data (fluorescent arbitrary units) are expressed as the mean ± SEM ($n = 6$ animals for all conditions; two-way ANOVA test followed by Bonferroni correction). (C) TCF20 expression decreases during gastrocnemius postnatal development. Representative Western blot and relative quantification of TCF20 expression at 0, 14, 35, and 70 post-natal days in total lysates of mouse gastrocnemius. Data (fluorescent arbitrary units) are expressed as the mean ± SEM, $n = 6$ animals for all conditions; ANOVA test followed by Tukey's multiple comparisons test; $^{**}p < 0.01$; $^{***}p < 0.001$; degrees of freedom between groups: 3; degrees of freedom within groups: 32; F-value: 8.80; p-value: 0.00021.

by confocal microscope, showed lower dendritic arborization in shTCF20 neurons compared to control neurons. This morphological alteration was prevented by co-transfection of shTCF20 with the shRNA-resistant construct (Resistant) (Figure 2A,B). Moreover, to evaluate the impact of TCF20 knockdown on dendritic spine formation, we analyzed the number, length,

and width of spines in shTCF20 rat cortical neuronal cultures. Analyses performed on images acquired by confocal microscopy showed a lower number of spines in shTCF20 neurons compared to neurons transfected with shSCR (Figure 2C,D). Co-transfection of shTCF20 with Resistant prevented the dendritic spine alterations. No differences in the spine length and width were detected in neurons transfected with shSCR, shTCF20, and shTCF20 + Resistant (Figure 2C,E,F). These data were also confirmed in neurons transfected at DIV7 and fixed at DIV10 (data not shown).

To further study the importance of TCF20 in modulating neuronal branching and spine morphology in vivo, we performed in utero electroporation (IUE) on wild-type mouse cortical neurons at embryonic day 14 (E14) with shSCR, shTCF20, or shTCF20 + Resistant constructs. Mice were

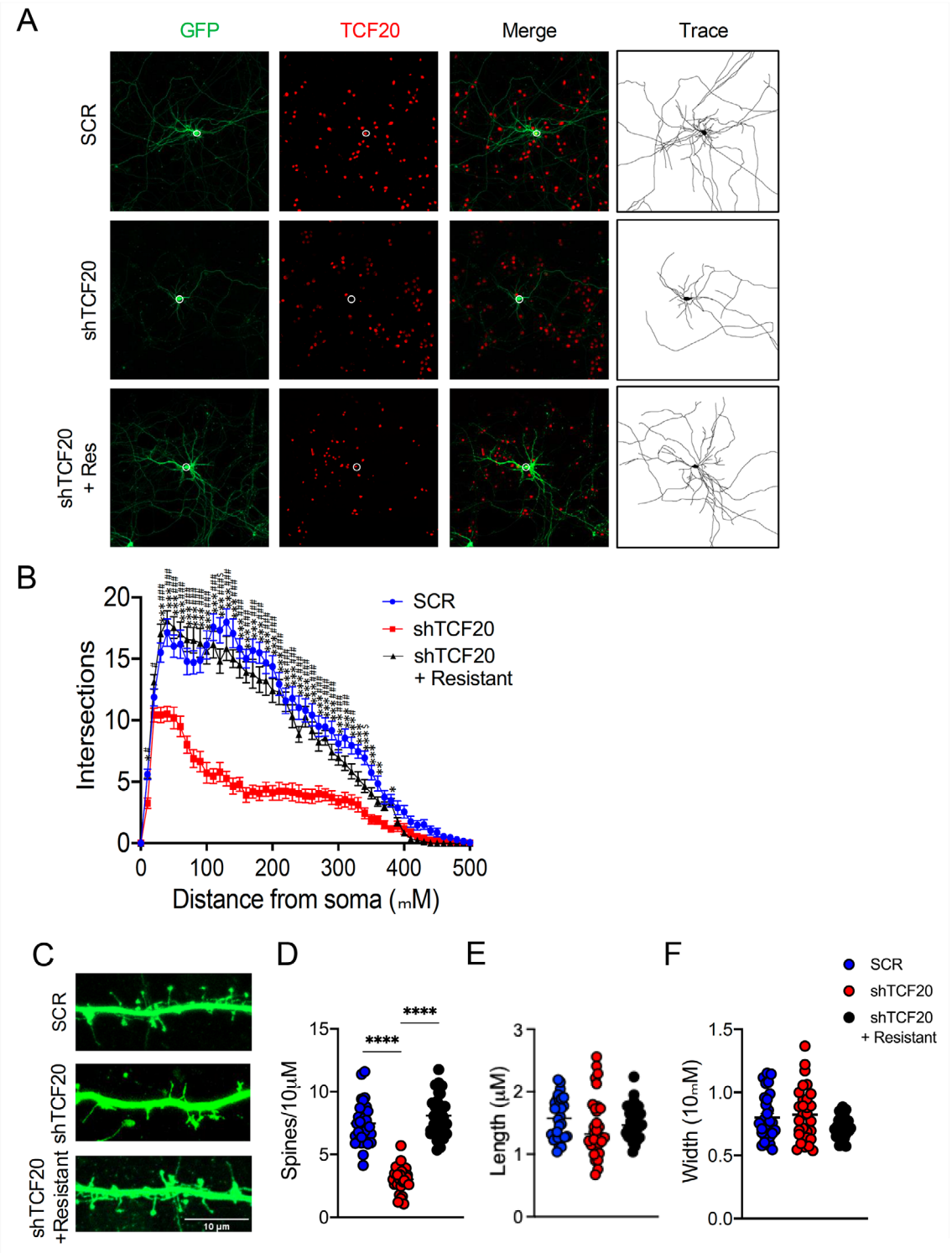

FIGURE 2 | Legend on next page.

FIGURE 2 | TCF20 knockdown reduces neuronal arborization and dendritic spine density. (A) Representative immunofluorescences images (20×) and relative traces of neuronal arborization in rat cortical neuronal cultures transfected with SCR, shTCF20, or shTCF20 + Resistant constructs. Scale bar 50 μM. (B) Results of Sholl analysis and quantification of the number of intersections, plotted against the distance from the soma. Data are expressed as the mean ± SEM ($n = 30$ individual neurons for each condition from three independent cultures; two-way ANOVA test followed by Bonferroni correction; *shTCF20 vs. SCR; #shTCF20 vs. Resistant; $SCR vs. Resistant; **$p < 0.01$; ***$p < 0.001$; ****$p < 0.0001$; #$p < 0.05$; ##$p < 0.01$; ###$p < 0.001$; $ $p < 0.05$); degrees of freedom between groups 2, degrees of freedom within groups 4647, *F*-value 247.67, *p*-value: 6.21e-103. (C) Representative images (63×) of neuronal spines in rat cortical neuronal cultures transfected with SCR, shTCF20, and shTCF20 + Resistant. (D–F) Quantification of dendritic spines number per 10 μM of dendrite (D), spines length (E) and spines width (F) in rat cortical neuronal cultures transfected with SCR, shTCF20, and shTCF20 + Resistant. Data are expressed as the mean ± SEM ($n = 30$ individual neurons for each condition from three independent cultures); statistical analysis: One-way ANOVA test followed by Tukey's multiple comparisons test; ****$p < 0.0001$; spines number, degrees of freedom between groups 2, degrees of freedom within groups 87, *F*-value 105.00, *p*-value: 6.38e-24; spines length, degrees of freedom between groups 2, degrees of freedom within groups: 87, *F*-value 0.89, *p*-value 0.416; spines width, degrees of freedom between groups 2, degrees of freedom within groups 87, *F*-value 2.60, *p*-value 0.080.

sacrificed at PND30, and brain slices were acquired by confocal microscopy. Also in vivo, branching analyses showed lower dendritic arborization in shTCF20 transfected neurons compared to shSCR or shTCF20 + Resistant transfected neurons (Figure 3A,B). In shTCF20 electroporated cortical neurons, we found not only a reduction in the number of spines but also lower spine length and width compared to dendritic spines in neurons expressing shSCR and shTCF20 + Resistant (Figure 3C–F).

3.3 | RNA-Sequencing Revealed Transcriptomic Alterations and a Downregulation of Pre- and Postsynaptic Pathways in TCF20 Knockdown Neurons

Since we found that TCF20 knockdown affected dendritic arborization and spine density, we decided to investigate the consequences of TCF20 silencing to identify differentially expressed genes (DEGs); we performed RNA-sequencing to investigate the transcriptome differences between rat cortical neuronal cultures transduced with a lentiviral construct expressing either shTCF20 or shSCR as a control. Neurons were transduced with shTCF20 or SCR lentiviruses at DIV4, and total RNA was extracted at DIV14. Approximately 16 000 distinct genes were identified, and 329 significantly changed after TCF20 knockdown: 116 were downregulated and 213 were upregulated (Figure 4A–D and Figure S2, Tables S1–S3). Among the downregulated proteins, we found genes involved in regulating neuronal morphogenesis and synapse such as BDNF, GRIN2B, Dlg4 (PSD-95), GABAralp1, and GABArap (Figure 4E).

Gene Ontology (GO) analysis revealed that the downregulated genes in shTCF20 neuronal cultures compared with SCR neuronal cultures were enriched in cellular components of synapse, in line with our findings of a lower number of spines in shTCF20 neurons, and in biological processes of anterograde transsynaptic signaling and neuropeptide signaling (Figure S3).

Considering that synaptic pathways are altered in shTCF20 neurons, we decided to conduct a SynGO analysis, an online analysis platform tool based on accumulated available research about synapse biology using GO annotations to novel ontology terms (Koopmans et al. 2019), which showed a significant downregulation in pre- and postsynaptic pathways (Figure S4).

3.4 | Molecular Analyses of Silenced TCF20 Cortical Neurons Confirmed Alterations of Specific Neuronal Proteins

Among the downregulated genes revealed by RNA-sequencing in rat cortical neuronal cultures transduced with shTCF20 or SCR lentiviruses, we focused our attention on relevant neuronal proteins involved in neuronal arborization, spine formation, and synaptic transmission. We analyzed, by WB, total lysates and synaptosomal preparations derived from rat cortical neuronal cultures transduced with shTCF20 or SCR lentiviruses at DIV4 and collected at DIV14.

In total homogenates of shTCF20 transduced neurons, we found a significant reduction in the expression levels of BDNF, PSD-95, c-Fos, and GABRA1 (Figure 5A). BDNF, c-Fos, and GABRA1 are included in the 116 statistically significant downregulated genes in our RNA-seq results. In synaptosomal preparation, the reduced expression of BDNF, PSD-95, and GABRA1 proteins was confirmed in shTCF20 transduced neurons, where we also found a significant reduction of GABRA5 and GluN2B (Figure 5B). The reduction of GluN2B was also found in the RNA-seq analysis (Figure 4E). Moreover, in synaptosomal preparations of shTCF20-transduced neurons, we found significantly increased expression of GluA2 in comparison with SCR-transduced neurons (Figure 5B).

3.5 | MEA Analysis Showed an Altered Synchronic Activity in Neurons in TCF20 Knockdown Rat Cortical Cultures

Since we observed a significant expression change of both GABAergic and glutamatergic receptors upon TCF20 knockdown, we asked whether this might also have an impact on the firing properties of cortical neurons. To this end, we recorded the electrophysiological activity of rat cortical cultures transduced with SCR or shTCF20 using a multielectrode

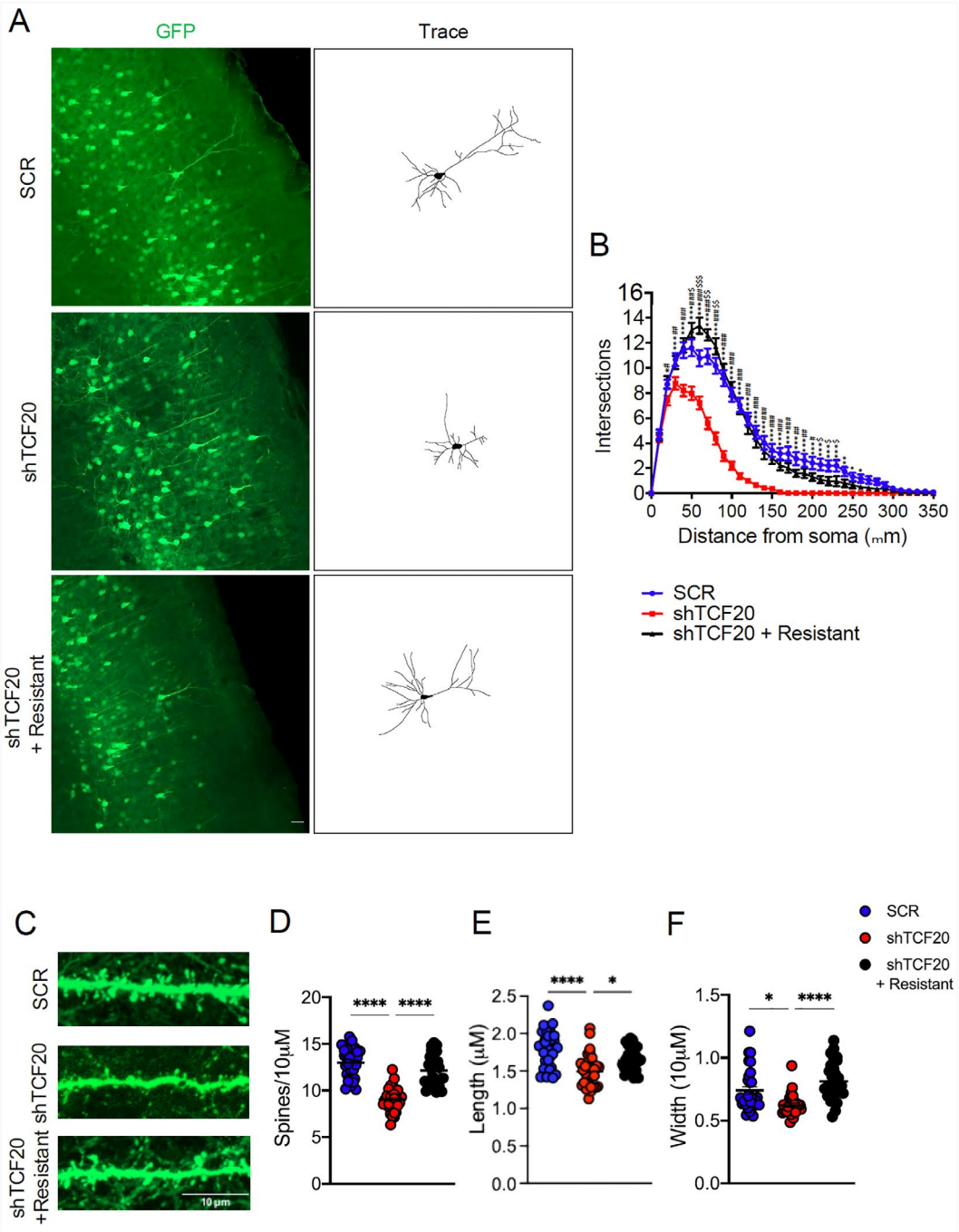

FIGURE 3 | TCF20 knockdown reduces neuronal arborization, dendritic spine density, length, and width of cortical mouse neurons. (A) Representative immunofluorescences images (20×) and relative traces of neuronal arborization in mouse cortical neurons in utero electroporated with SCR, shTCF20, or shTCF20 + Resistant constructs. Scale bar 100 µM. (B) Results of Sholl analysis and quantification of the number of intersections, plotted against the distance from the soma. Data are expressed as the mean ± SEM ($n = 30$ individual neurons for each condition from three independent animals; two-way ANOVA test followed by Bonferroni correction; *shTCF20 vs. SCR; #shTCF20 vs. Resistant; $SCR vs. Resistant; *$p < 0.05$; **$p < 0.01$; ***$p < 0.001$; # $p < 0.05$; ## $p < 0.01$; ### $p < 0.001$; $ $p < 0.05$; $$ $p < 0.01$; $$$ $p < 0.001$); degrees of freedom between groups 2, degrees of freedom within groups 359, F-value 98.51, p-value: 2.24e-42. (C) Representative images (63×) of neuronal spines in mouse cortical neurons in utero electroporated with SCR, shTCF20, and shTCF20 + Resistant constructs. (D–F) Quantification of dendritic spines number per 10 µM of dendrite (D), spines length (E) and spines width (F) in mouse cortical neurons transfected with SCR, shTCF20, and shTCF20 + Resistant constructs. Data are expressed as the mean ± SEM ($n = 30$ individual neurons for each condition from three independent animals; one-way ANOVA test followed by Tukey's multiple comparisons test; *$p < 0.05$; ****$p < 0.0001$); spines number, degrees of freedom between groups 2, degrees of freedom within groups 87, F-value 56.13, p-value: 2.21e-16; spines length, degrees of freedom between groups 2, degrees of freedom within groups: 87, F-value 14.95, p-value 2.63e-06; spines width, degrees of freedom between groups 2, degrees of freedom within groups 87, F-value 14.44, p-value 3.85e-06.

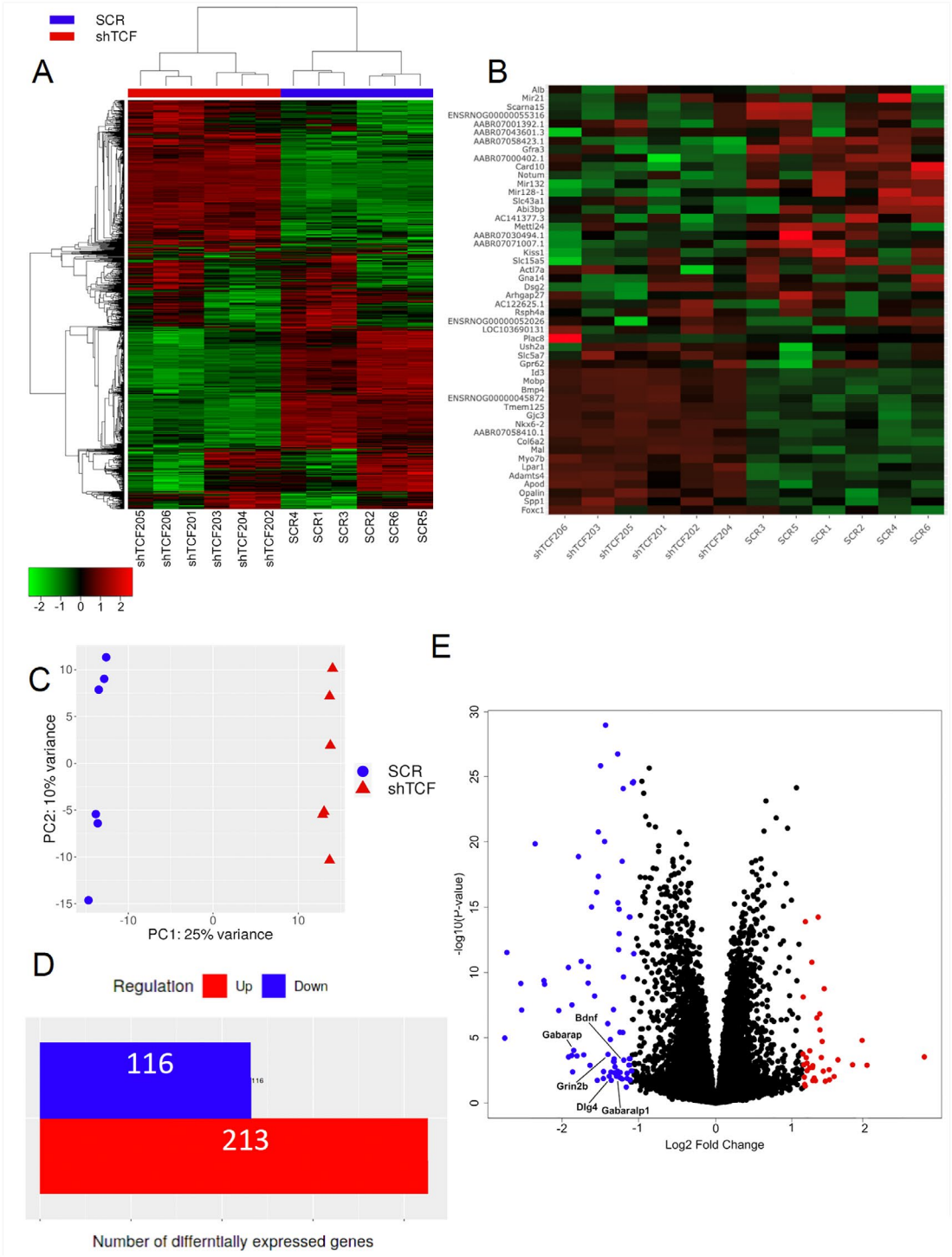

FIGURE 4 | RNA-sequencing analyses. (A, B) Heatmap of the identified DEGs (hierarchical clustering, Pearson correlation, average function linkage and 4 as cut-off z-score) where a clear clustering of the control samples (SCR) over the shTCF20 is visible. (C) Principal component analysis shows a simple separation by the first principal component which explains 25% of the total variance between the SCR and shTCF20 group. (D) Differential gene expression analysis (DESeq2 method) reveals 116 downregulated and 213 upregulated genes in the SCR versus shTCF20 contrast. (E) Volcano plot evidencing relevant down-expressing genes like Dlg4, BDNF, GABARAP, GRIN2b, and Gabaralp1.

array (MEA) system. We observed a significant reduction in the burst frequency and percentage of spikes recorded within bursts in comparison to SCR transduced neurons. These data indicated that a loss of TCF20 might result in an increased non-synchronic activity in primary cultures (Figure 6A,B).

3.6 | Neurons Transfected With TCF20 Mutants Showed Lower Dendritic Arborization and Spine Density

Recently, several mutations have been reported in patients affected by TAND syndrome (Babbs et al. 2014; Schäfgen

et al. 2016; Lelieveld et al. 2016; Torti et al. 2019; Vetrini et al. 2019; Study 2017). To investigate possible morphological consequences due to these mutations in neurons, we generated putative TCF20 mutants, fused to green fluorescent protein (GFP), that mimic the reported nonsense mutations c.955C>T and c.5719C>T (Study 2017; Schäfgen et al. 2016). 955C>T mutation leads to a protein of 318 amino acids truncated at the beginning of exon 2 whereas 5719C>T mutation leads to a protein of 1906 amino acids truncated at exon 3. During the subcloning of 5719C>T mutation, we generated an intermediate construct, which was used in our experiments, coding for half protein and composed of 1079 amino acids until nucleotide 3237 (Figure S5).

GFP-TCF20, GFP-318-TCF20, GFP-1079-TCF20, and GFP-1906-TCF20 constructs were transfected in cortical neurons in order to study their localization. We found that even if some of them

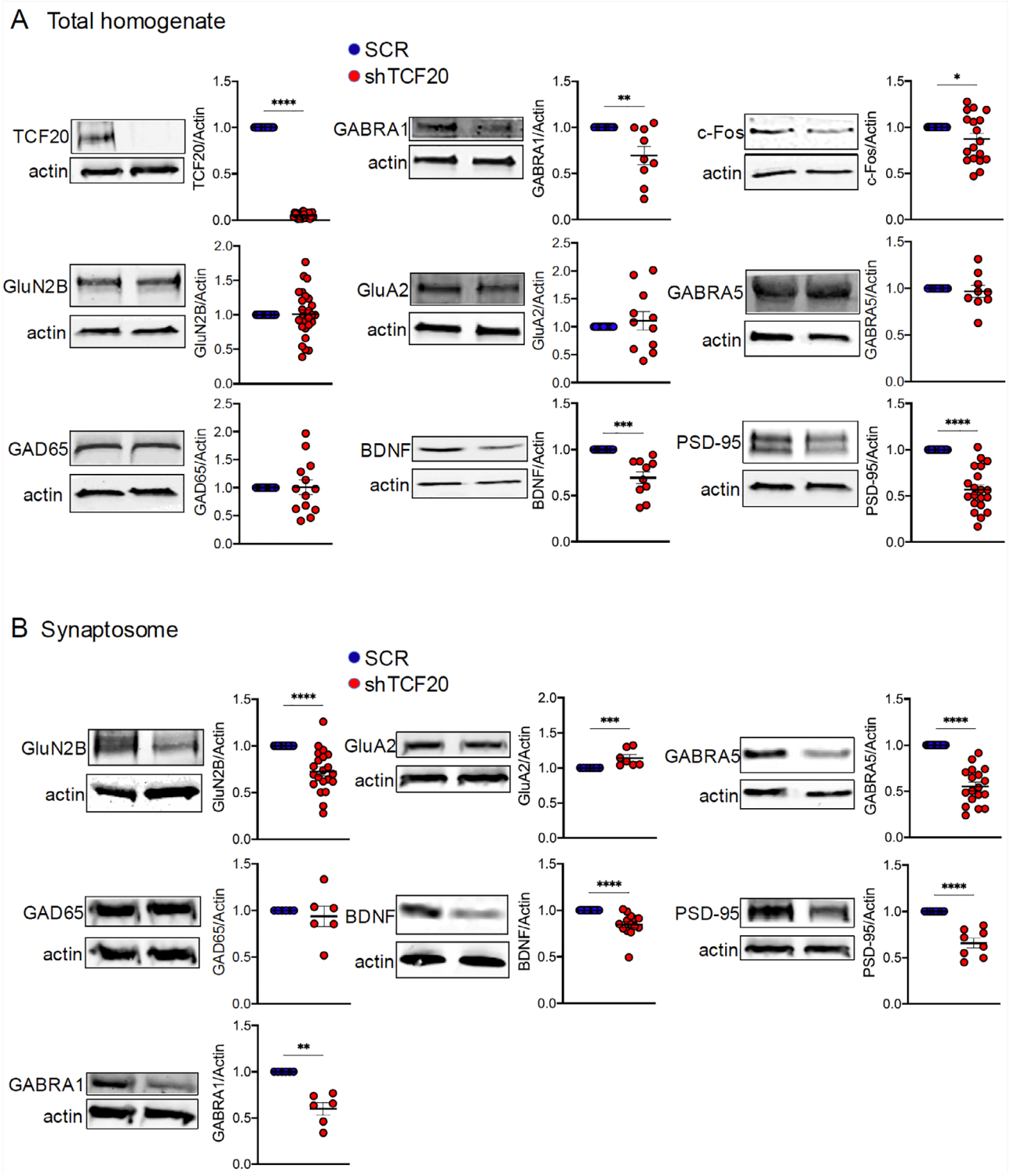

FIGURE 5 | Legend on next page.

FIGURE 5 | TCF20 knockdown alters neuronal proteins expression in total lysate and in synaptosomal fraction. (A) Representative Western blot and relative quantification of total lysate from shTCF20 or SCR transduced cortical neurons. Data are expressed as the mean ± SEM (2–3 mixed 6-well plates obtained from $n = 12$ independent cultures; one-sample t test; *$p < 0.05$; **$p < 0.01$; ***$p < 0.001$; ****$p < 0.0001$). Statistical analysis: TCF20 degrees of freedom 26, t value 31.66, p value 2.71e-22; GABRA1 degrees of freedom 16, t value 3.09, p value 0.0070; c-FOS degrees of freedom 34, t value 2.08, p value 0.0454; GluN2B degrees of freedom 50, t value −0.105, p value 0.917; GluA2 degrees of freedom 20, t value −0.64, p value 0.530; GABRA5 degrees of freedom 16, t value −0.46, p value 0.650; GAD65 degrees of freedom 24, t value −0.072, p value 0.943; BDNF degrees of freedom 18, t value 4.72, p value 0.00017; PSD-95° of freedom 44, t value 4.50, p value 4.88e-05. (B) Representative Western blot and relative quantification of synaptosomal preparation from shTCF20 or SCR transduced cortical neurons. Data are expressed as the mean ± SEM (2–3 mixed 6-well plates obtained from $n = 9$ independent cultures; one-sample t test; **$p < 0.01$; ***$p < 0.001$; ****$p < 0.0001$). Statistical analysis: GluN2B degrees of freedom 40, t value 4.72, p value 0.00000168; GluA2 degrees of freedom 14, t value −2.44, p value 0.0284; GAD65 degrees of freedom 10, t value 0.55, p value 0.5945; BDNF degrees of freedom 28, t value 4.41, p value 0.00014; PSD-95° of freedom 14, t value 6.53, p value 0.0000134; GABRA1 degrees of freedom 10, t value 5.90, p value 0.00015.

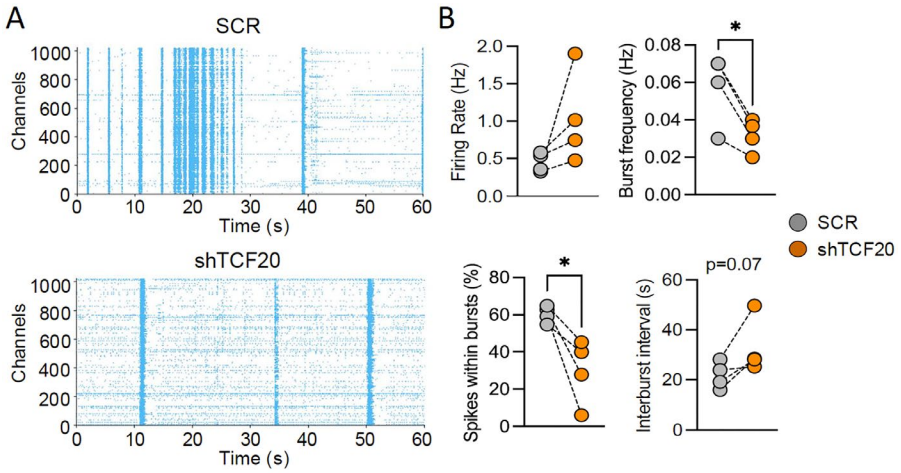

FIGURE 6 | Neuronal activity registered with MEA is reduced in shTCF20 transduced neurons compared with SCR transduced neurons. (A) Representative raster plot in SCR (upper panel) and shTCF20 recorded cultures (lower panel). (B) Analysis of firing rate, burst frequency, percentage of spikes within bursts and duration of inter-burst interval ($n = 4$ independent cultures, sample t test *$p < 0.01$ vs. SCR); firing rate, degrees of freedom 6, t value 1.621, p value 0.18; burst frequency, degrees of freedom 6, t value 3.36, p value 0.021; spikes within bursts, degrees of freedom 6, t value 2.63, p value 0.043; interburst interval, degrees of freedom 6, t value 2.83, p value 0.07.

are localized in the cytoplasm; all of them are also localized to the nucleus indicating that even if these mutants express only part of the protein; they might interfere with the transcriptional activity of TCF20 (Figure S6).

To investigate possible alterations in dendritic arborization and spine density due to mutants or TCF20 overexpression, rat cortical neuronal cultures were co-transfected with GFP-318-TCF20, GFP-1079-TCF20, GFP-1906-TCF20, or GFP-TCF20 plus TdTomato at DIV7 and fixed at DIV14. Dendrite morphology of transfected neurons was then evaluated by Sholl analysis on images acquired by confocal microscope. Our analyses showed a significantly lower dendritic arborization in neurons transfected with the three mutants but also overexpressing TCF20 in comparison with control neurons transfected with TdTomato (Figure 7A,B).

Finally, we analyzed the number, length, and width of spines in rat cortical neuronal cultures co-transfected with GFP-318-TCF20, GFP-1079-TCF20, GFP-1906-TCF20, or GFPTCF20 plus TdTomato at DIV7 and fixed at DIV14. Neurons transfected with the three mutants but also overexpressing TCF20 in comparison with control neurons transfected with TdTomato displayed a significantly lower number of spines. No differences in the length and width of all described conditions were detected (Figure 7C–F).

4 | Discussion

In this study, we have demonstrated that TCF20 is a crucial protein in neuronal development and function, as it regulates the expression of proteins that are important for synapse formation and neuronal development. Recent data have suggested that TCF20 plays a significant role in neurogenesis as TCF20 knockout mice exhibit neurogenesis defects and autistic-like behavioral patterns. Depletion of TCF20 in neuronal precursors has been found to decrease neuronal differentiation and increase neuronal precursor proliferation, which could be responsible for abnormal behaviors (Feng et al. 2020). In a more recent study, TCF20 has been identified as a functional and molecular partner of MeCP2, indicating that the MeCP2-TCF20 complex may play a role in regulating neuronal development and brain function, possibly by controlling the expression of BDNF (Zhou et al. 2022).

However, it is not yet clear if and how TCF20 modulates neuronal development after birth, and whether altered postnatal

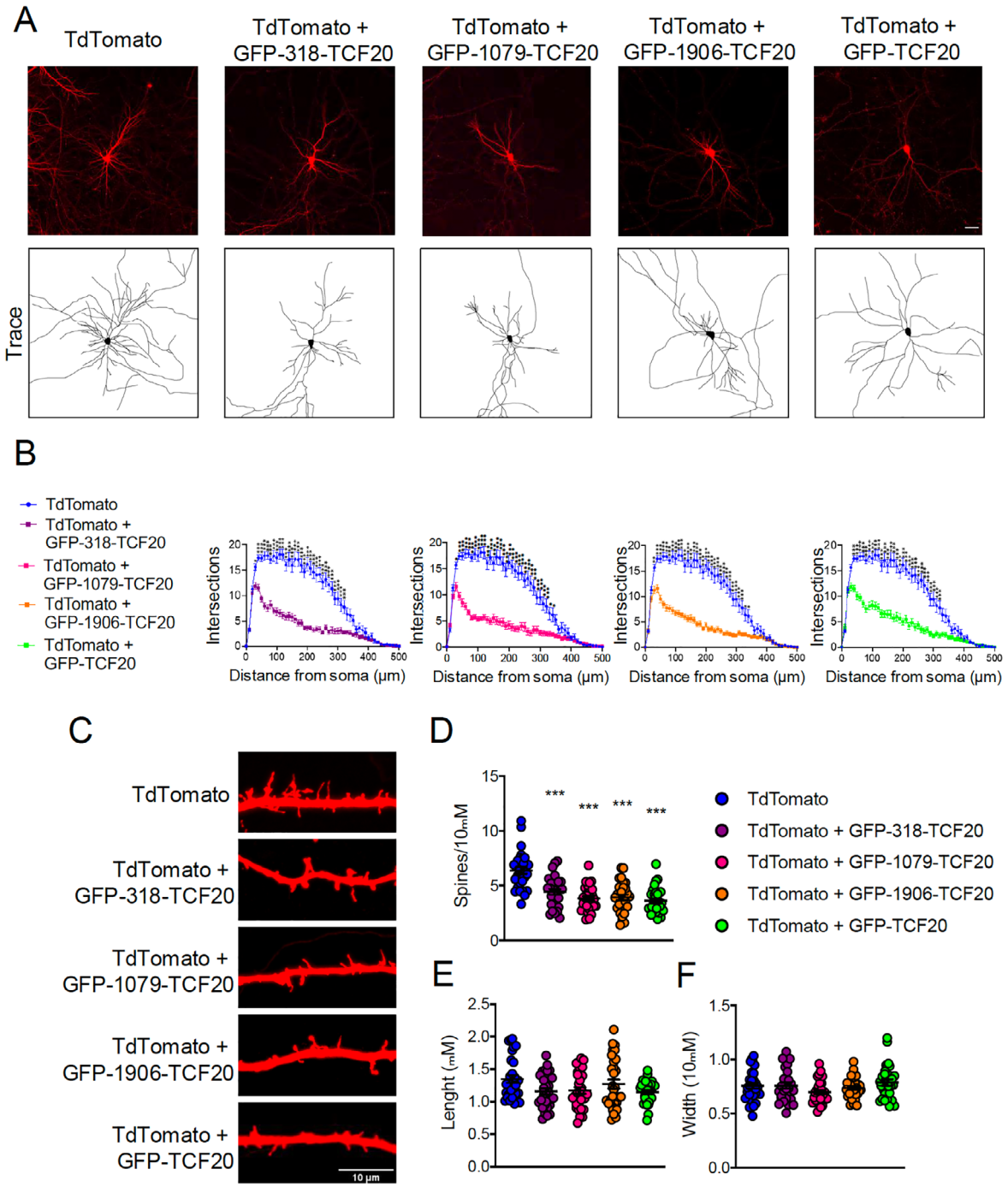

FIGURE 7 | Neurons transfected with TCF20 mutants or GFP-TCF20 show a reduced neuronal arborization and dendritic spine density with no significant differences in spine length and width. (A) Representative immunofluorescences images (20×) of neuronal arborization and relative traces of rat cortical neuronal cultures transfected with TdTomato, TdTomato + GFP-318-TCF20, TdTomato + GFP-1079-TCF20, TdTomato + GFP-1906-TCF20, or TdTomato + GFP-TCF20. Scale bar 50 μM. (B) Results of Sholl analysis and quantification of the number of intersections, plotted against the distance from the soma. Data are expressed as the mean ± SEM ($n = 30$ individual neurons for each condition from three independent cultures; two-way ANOVA test followed by Bonferroni correction; $^{*}p < 0.01$; $^{**}p < 0.001$, $^{***}p < 0.0001$ vs. TdTomato); TCF20, degrees of freedom 2998, t value 22.26, p value 1.10e-101; 955-TCF20, degrees of freedom 3058, t value 24.19, p value 1.98e-118; 3237-TCF20, degrees of freedom 3058, t value 25.47, p value 5.60e-130; 5719-TCF20, degrees of freedom 3058, t value 25.47, p value 5.60e-130. (C) Representative images (63×) of neuronal spines in rat cortical neuron cultures transfected with TdTomato, TdTomato + GFP-318-TCF20, TdTomato + GFP-1079-TCF20, TdTomato + GFP-1906-TCF20, or TdTomato + GFP-TCF20. (D–F) Quantification of dendritic spines number per 10 μM of dendrite (D), spines length (E), and spines width (F) in rat cortical neuron cultures co-transfected with TdTomato and mutants or overexpressing TCF20. Data are expressed as the mean ± SEM ($n = 30$ individual neurons for each condition from three independent cultures); one-way ANOVA test followed by Tukey's multiple comparisons test; $^{***}p < 0.001$; spines number, degrees of freedom between groups 4, degrees of freedom within groups: 145, F-value: 20.45, p-value: 1.99e-13; spines length, degrees of freedom between groups 4, degrees of freedom within groups: 145; F-value: 2.60; p-value: 0.0387; spines width, degrees of freedom between groups 4, degrees of freedom within groups: 145; F-value: 1.90; p-value: 0.114.

neuronal development may also cause TAND syndrome. Given this background, we conducted an investigation to determine the role of TCF20 in postnatal neuronal function.

We found that TCF20 is expressed in mature brain, suggesting that it may also have an important function in mature neurons. Therefore, it is essential to fully understand the role of TCF20 in synapse and neuronal circuit formation, which are the main molecular pathogenic causes of ID and ASD (Verpelli and Sala 2012). Analysis of TCF20 expression in various adult mouse brain regions confirmed its expression in the hippocampus, striatum, cerebral cortex, and cerebellum, which are areas mainly involved in neurodevelopmental disorders (Jiang and Ehlers 2013). We found no differential expression in these areas between male and female mice (see Figure 1).

After confirming that TCF20 is ubiquitously expressed in the brain and knowing that TCF20 mutations lead to a developmental disorder, we evaluated its expression during mouse brain development at 0, 14, 35, and 70 post-natal days (PND) in total homogenates. TCF20 expression was significantly increased from PND0 to PND70, confirming its importance during development and after birth (see Figure 1). Since patients with TAND syndrome present hypotonia, we analyzed TCF20 expression during mouse gastrocnemius post-natal development at 0, 14, 35, and 70 PND (Schäfgen et al. 2016; Torti et al. 2019; Vetrini et al. 2019). The protein expression decreased from PND0 to PND70, with a stronger decrease from PND0 to PND14, suggesting a role of TCF20 in the early stage of muscle growth and development (see Figure 2).

Thus, our data suggest a different role of TCF20 in the brain compared to its role in muscle. While in the brain TCF20 is required for postnatal neuronal development, in the muscle it is probably crucial before birth, as its expression almost disappears a few days after birth. However, the role of TCF20 in muscle remains to be determined.

A major focus of our study was to investigate the physiological function of TCF20 in neurons. Given that alterations in neuronal morphology are often associated with ASDs (Verpelli and Sala 2012; Dang et al. 2018), we examined the impact of TCF20 silencing on neuronal phenotype in vitro. Our results indicated that cortical neurons silenced for TCF20 exhibited reduced dendritic arborization and spine density (Figure 2). To confirm these findings in vivo, we also conducted morphological studies in mouse cortical neurons that were electroporated with shTCF20. Similarly, cortical neurons silenced for TCF20 exhibited a reduction in dendritic branching complexity, spine density, length, and width (Figure 3).

These observations suggest that TCF20 expression is essential for proper neuronal maturation and synaptic connectivity. To further investigate TCF20 function, we performed RNA-sequencing in cortical cultures that were transduced with shTCF20 lentivirus and compared them to cortical cultures transduced with SCR lentivirus. We identified 329 significantly changed genes in shTC20 cultures. GO analysis revealed that in shTCF20 rat cortical neurons, downregulated genes were enriched in cellular components of synapse and in biological processes of anterograde trans-synaptic signaling and neuropeptide signaling (Extended Data Figure 4–2). SynGO analysis (Koopmans et al. 2019) showed a significant downregulation in pre- and postsynaptic pathways for cellular compartments and biological processes (Extended Data Figure 4–3).

Based on these results, we analyzed the expression of neuronal proteins in TCF20-deficient neurons and found decreased levels of GABRA1, BDNF, PSD-95, and c-Fos in total homogenates (Figure 5) and in synaptosomal preparations (Figure 5) of shTCF20 rat cortical cultures. Additionally, GluN2B and GABRA5 were significantly downregulated, and GluA2 was significantly upregulated in synaptosomal preparations of shTCF20 rat cortical cultures (Figure 5).

PSD-95 is one of the most abundant proteins of the postsynaptic density (Walikonis et al. 2000) and is well-known to promote synapse maturation and stability, synaptic strength, and plasticity (El-Husseini et al. 2000; Elias et al. 2006). PSD-95 can directly interact with GluN2B (Kornau et al. 1995; Kim et al. 1996), an NMDA receptor that, when phosphorylated, affects the recruitment of other NMDA receptors, regulating their trafficking and synaptic localization to maintain their activation (Qiu, Li, and Zhuo 2011). We speculate that the reduction of PSD-95 and GluN2B in shTCF20 neurons may lead to a reduction in NMDA receptor function and impaired synaptic plasticity, also confirmed by the lower spine number observed in shTCF20 neurons. The reduced number of dendritic spines might be due to an impairment in formation or in the maintaining of the spines. Thus, future experiments should better define the specific role or TCF20 in regulating the number of dendritic spines.

c-Fos is an immediate-early gene (IEG) that encodes a transcription factor induced by neuronal activity, particularly after calcium influx through NMDA receptors and L-type voltage-sensitive calcium channels (VSCC) (Chaudhuri et al. 2000). Because c-Fos protein is a neuronal activity marker induced by NMDARs (Liste et al. 1995; Parthasarathy and Graybiel 1997), we could speculate that its lower expression, demonstrated in shTCF20 neurons, is due to a low level of NMDARs. Moreover, it was demonstrated that c-Fos regulates the expression of BDNF, mediating neuronal excitability and survival (Zhang et al. 2002). Indeed, BDNF is well-known to promote neuronal differentiation by stimulating neurite outgrowth and synapse (Alsina, Vu, and Cohen-Cory 2001; Bamji et al. 2006; Verpelli et al. 2010); in our shTCF20 neurons, BDNF downregulation is in line with the altered dendritic and spine phenotype.

GluA2 is an AMPA receptor subunit that plays an important role in excitatory synaptic transmission (Isaac, Ashby, and McBain 2007; Bassani et al. 2009). On the other hand, gamma-aminobutyric acid type A (GABAA) receptors, such as GABRA1 and GABRA5, are known to mainly mediate fast inhibitory neurotransmission in response to gamma-aminobutyric acid (GABA), the major inhibitory neurotransmitter in the mammalian brain (Johnston 2005). Because GluA2 is upregulated and GABRA1 and GABRA5 are downregulated, we expected hyperexcitability in neurons deficient for TCF20.

For this reason, we conducted a MEA assay, which showed a tendency towards increased firing rates in shTCF20 cultures, and a reduced percentage of spikes recorded within bursts

(Figure 6). These results suggest that the loss of TCF20 may result in increased non-synchronous activity in primary culture, and a lack of coordination of global activity, which may be due to lower dendritic arborization and a lower number of spines in shTCF20 neurons. As a result, the neurons may not be able to create a proper synaptic network.

To better understand the impact of TCF20 mutations reported in patients, we overexpressed mutant forms of the protein in rat neuronal cultures. Like the downregulation of TCF20, mutant forms lead to a decrease in neuronal dendrite arborization and dendritic spine density, which is a neuronal phenotype that may be present in TAND syndrome patients. Interestingly, overexpression of the wild-type form of TCF20 also leads to the same phenotype observed in TCF20-silenced, overexpressing, or mutant neurons. These findings suggest that the appropriate protein level is crucial to ensure proper neuronal development (Figure 7).

Taken together, our results suggest that TCF20 plays a central and critical role in the arborization of cortical neurons and the formation of dendritic spines. These morphological alterations may be mediated by the impaired expression pattern of synaptic proteins found in TCF20 knockdown cortical neurons. However, further analysis is needed to better understand the specific molecular mechanism underlying these morphological alterations and to correlate them with the pathogenesis of TAND syndrome in human patients.

Author Contributions

Ersilia Vinci: methodology, writing – original draft, conceptualization, investigation. **Stefania Beretta:** methodology, investigation. **Veronica Colombo:** methodology, investigation. **Antonio Zippo:** investigation, methodology, data curation. **Alberto Catanese:** methodology, data curation. **Christoph Wiegreffe:** methodology. **Stefan Britsch:** methodology. **Tobias Boeckers:** conceptualization, funding acquisition. **Chiara Verpelli:** conceptualization, supervision, funding acquisition. **Carlo Sala:** conceptualization, funding acquisition, methodology, project administration, supervision.

Acknowledgments

This work was supported by Fondation Jerome Lejeune (project # 2054-SC2021A to C.S. and project #1938 to C.V.), the Comitato Telethon Fondazione Onlus (grant no. GMR22T1061 to C.S.) and Else Kröner Foundation to T.B. Italian Ministry of University and Research (MUR), support under the National Recovery and Resilience Plan (NRRP), P2022374Y9_ LS5 (to C.V.). Open access publishing facilitated by Consiglio Nazionale delle Ricerche, as part of the Wiley - CRUI-CARE agreement.

Conflicts of Interest

C.S. is a handling Editor for the *Journal of Neurochemistry*, and the guest Editor of the Autism Spectrum Disorder Special Issue. The other authors declare no conflicts of interest.

Data Availability Statement

The data that support the findings of this study are available from the corresponding author upon reasonable request.

Peer Review

The peer review history for this article is available at https://www.webofscience.com/api/gateway/wos/peer-review/10.1111/jnc.16297.

References

Alsina, B., T. Vu, and S. Cohen-Cory. 2001. "Visualizing Synapse Formation in Arborizing Optic Axons In Vivo: Dynamics and Modulation by BDNF." *Nature Neuroscience* 4, no. 11: 1093–1101.

Babbs, C., D. Lloyd, A. T. Pagnamenta, et al. 2014. "De Novo and Rare Inherited Mutations Implicate the Transcriptional Coregulator TCF20/SPBP in Autism Spectrum Disorder." *Journal of Medical Genetics* 51, no. 11: 737–747.

Bamji, S. X., B. Rico, N. Kimes, and L. F. Reichardt. 2006. "BDNF Mobilizes Synaptic Vesicles and Enhances Synapse Formation by Disrupting Cadherin-Beta-Catenin Interactions." *Journal of Cell Biology* 174, no. 2: 289–299.

Bassani, S., P. Valnegri, F. Beretta, and M. Passafaro. 2009. "The GLUR2 Subunit of AMPA Receptors: Synaptic Role." *Neuroscience* 158, no. 1: 55–61.

Bowling, K. M., M. L. Thompson, M. D. Amaral, et al. 2017. "Genomic Diagnosis for Children With Intellectual Disability and/or Developmental Delay." *Genome Medicine* 9, no. 1: 43.

Chaudhuri, A., S. Zangenehpour, F. Rahbar-Dehgan, and F. Ye. 2000. "Molecular Maps of Neural Activity and Quiescence." *Acta Neurobiologiae Experimentalis (Wars)* 60, no. 3: 403–410.

Chen, Y., B. Stevens, J. Chang, J. Milbrandt, B. A. Barres, and J. W. Hell. 2008. "NS21: Re-Defined and Modified Supplement B27 for Neuronal Cultures." *Journal of Neuroscience Methods* 171, no. 2: 239–247.

Dang, T., W. Y. Duan, B. Yu, et al. 2018. "Autism-Associated Dyrk1a Truncation Mutants Impair Neuronal Dendritic and Spine Growth and Interfere With Postnatal Cortical Development." *Molecular Psychiatry* 23, no. 3: 747–758.

Darvekar, S., S. S. Johnsen, A. B. Eriksen, T. Johansen, and E. Sjøttem. 2012. "Identification of Two Independent Nucleosome-Binding Domains in the Transcriptional Co-Activator SPBP." *Biochemical Journal* 442, no. 1: 65–75.

Deciphering Developmental Disorders Study. 2017. "Prevalence and Architecture of De Novo Mutations in Developmental Disorders." *Nature* 542, no. 7642: 433–438.

El-Husseini, A. E., E. Schnell, D. M. Chetkovich, R. A. Nicoll, and D. S. Bredt. 2000. "PSD-95 Involvement in Maturation of Excitatory Synapses." *Science* 290, no. 5495: 1364–1368.

Elias, G. M., L. Funke, V. Stein, S. G. Grant, D. S. Bredt, and R. A. Nicoll. 2006. "Synapse-Specific and Developmentally Regulated Targeting of AMPA Receptors by a Family of MAGUK Scaffolding Proteins." *Neuron* 52, no. 2: 307–320.

Feng, C., J. Zhao, F. Ji, L. Su, Y. Chen, and J. Jiao. 2020. "TCF20 Dysfunction Leads to Cortical Neurogenesis Defects and Autistic-Like Behaviors in Mice." *EMBO Reports* 21, no. 8: e49239.

Gburcik, V., N. Bot, M. Maggiolini, and D. Picard. 2005. "SPBP is a Phosphoserine-Specific Repressor of Estrogen Receptor Alpha." *Molecular and Cellular Biology* 25, no. 9: 3421–3430.

Gray, P. A., H. Fu, P. Luo, et al. 2004. "Mouse Brain Organization Revealed Through Direct Genome-Scale TF Expression Analysis." *Science* 306, no. 5705: 2255–2257.

Isaac, J. T., M. C. Ashby, and C. J. McBain. 2007. "The Role of the GluR2 Subunit in AMPA Receptor Function and Synaptic Plasticity." *Neuron* 54, no. 6: 859–871.

Jiang, Y. H., and M. D. Ehlers. 2013. "Modeling Autism by SHANK Gene Mutations in Mice." *Neuron* 78, no. 1: 8–27.

Johnston, G. A. 2005. "GABA(A) Receptor Channel Pharmacology." *Current Pharmaceutical Design* 11, no. 15: 1867–1885.

Kim, E., K.-O. Cho, A. Rothschild, and M. Sheng. 1996. "Heteromultimerization and NMDA Receptor-Clustering Activity of Chapsyn-110, a Member of the PSD-95 Family of Proteins." *Neuron* 17: 103–113.

Koopmans, F., P. van Nierop, M. Andres-Alonso, et al. 2019. "SynGO: An Evidence-Based, Expert-Curated Knowledge Base for the Synapse." *Neuron* 103, no. 2: 217–234.e4.

Kornau, H.-C., L. T. Schenker, M. B. Kennedy, and P. H. Seeburg. 1995. "Domain Interaction Between NMDA Receptor Subunits and the Postsynaptic Density Protein PSD-95." *Science* 269: 1737–1740.

Kurtas, N., F. Arrigoni, E. Errichiello, et al. 2018. "Chromothripsis and Ring Chromosome 22: A Paradigm of Genomic Complexity in the Phelan-McDermid Syndrome (22q13 Deletion Syndrome)." *Journal of Medical Genetics* 55, no. 4: 269–277.

Lein, E. S., M. J. Hawrylycz, N. Ao, et al. 2007. "Genome-Wide Atlas of Gene Expression in the Adult Mouse Brain." *Nature* 445, no. 7124: 168–176.

Lelieveld, S. H., M. R. Reijnders, R. Pfundt, et al. 2016. "Meta-Analysis of 2,104 Trios Provides Support for 10 New Genes for Intellectual Disability." *Nature Neuroscience* 19, no. 9: 1194–1196.

Liste, I., G. Rozas, M. J. Guerra, and J. L. Labandeira-Garcia. 1995. "Cortical Stimulation Induces Fos Expression in Striatal Neurons via NMDA Glutamate and Dopamine Receptors." *Brain Research* 700, no. 1–2: 1–12.

Lois, C., E. J. Hong, S. Pease, E. J. Brown, and D. Baltimore. 2002. "Germline Transmission and Tissue-Specific Expression of Transgenes Delivered by Lentiviral Vectors." *Science* 295, no. 5556: 868–872.

Lyngsø, C., G. Bouteiller, C. K. Damgaard, et al. 2000. "Interaction Between the Transcription Factor SPBP and the Positive Cofactor RNF4. An Interplay Between Protein Binding Zinc Fingers." *Journal of Biological Chemistry* 275, no. 34: 26144–26149.

Montani, C., M. Ramos-Brossier, L. Ponzoni, et al. 2017. "The X-Linked Intellectual Disability Protein IL1RAPL1 Regulates Dendrite Complexity." *Journal of Neuroscience* 37, no. 28: 6606–6627.

Mossa, A., J. Pagano, L. Ponzoni, et al. 2021. "Developmental Impaired Akt Signaling in the Shank1 and Shank3 Double Knock-Out Mice." *Molecular Psychiatry* 26: 1928–1944.

Naldini, L., U. Blomer, P. Gallay, et al. 1996. "In Vivo Gene Delivery and Stable Transduction of Nondividing Cells by a Lentiviral Vector." *Science* 272, no. 5259: 263–267.

Osborn, M., and K. Weber. 1982. "Immunofluorescence and Immunocytochemical Procedures With Affinity Purified Antibodies: Tubulin-Containing Structures." *Methods in Cell Biology* 24: 97–132.

Parthasarathy, H. B., and A. M. Graybiel. 1997. "Cortically Driven Immediate-Early Gene Expression Reflects Modular Influence of Sensorimotor Cortex on Identified Striatal Neurons in the Squirrel Monkey." *Journal of Neuroscience* 17, no. 7: 2477–2491.

Phelan, K., and H. E. McDermid. 2012. "The 22q13.3 Deletion Syndrome (Phelan-McDermid Syndrome)." *Molecular Syndromology* 2, no. 3–5: 186–201.

Phelan, M. C. 2008. "Deletion 22q13.3 Syndrome." *Orphanet Journal of Rare Diseases* 3: 14.

Qiu, S., X. Y. Li, and M. Zhuo. 2011. "Post-Translational Modification of NMDA Receptor GluN2B Subunit and Its Roles in Chronic Pain and Memory." *Seminars in Cell & Developmental Biology* 22, no. 5: 521–529.

Rekdal, C., E. Sjøttem, and T. Johansen. 2000. "The Nuclear Factor SPBP Contains Different Functional Domains and Stimulates the Activity of Various Transcriptional Activators." *Journal of Biological Chemistry* 275, no. 51: 40288–40300.

Sala, C., C. Vicidomini, I. Bigi, A. Mossa, and C. Verpelli. 2015. "Shank Synaptic Scaffold Proteins: Keys to Understanding the Pathogenesis of Autism and Other Synaptic Disorders." *Journal of Neurochemistry* 135, no. 5: 849–858.

Sanz, L., J. Moscat, and M. T. Diaz-Meco. 1995. "Molecular Characterization of a Novel Transcription Factor That Controls Stromelysin Expression." *Molecular and Cellular Biology* 15, no. 6: 3164–3170.

Schäfgen, J., K. Cremer, J. Becker, et al. 2016. "De Novo Nonsense and Frameshift Variants of TCF20 in Individuals With Intellectual Disability and Postnatal Overgrowth." *European Journal of Human Genetics* 24, no. 12: 1739–1745.

Sjøttem, E., C. Rekdal, G. Svineng, et al. 2007. "The ePHD Protein SPBP Interacts With TopBP1 and Together They Co-Operate to Stimulate Ets1-Mediated Transcription." *Nucleic Acids Research* 35, no. 19: 6648–6662.

Smeland, O. B., O. Frei, K. Kauppi, et al. 2017. "Identification of Genetic Loci Jointly Influencing Schizophrenia Risk and the Cognitive Traits of Verbal-Numerical Reasoning, Reaction Time, and General Cognitive Function." *JAMA Psychiatry* 74, no. 10: 1065–1075.

Sommer, D., S. Rajkumar, M. Seidel, et al. 2022. "Aging-Dependent Altered Transcriptional Programs Underlie Activity Impairments in Human C9orf72-Mutant Motor Neurons." *Frontiers in Molecular Neuroscience* 15: 894230.

Torti, E., B. Keren, E. E. Palmer, et al. 2019. "Variants in TCF20 in Neurodevelopmental Disability: Description of 27 New Patients and Review of Literature." *Genetics in Medicine* 21, no. 9: 2036–2042.

Upadia, J., P. R. Gonzales, T. P. Atkinson, et al. 2018. "A Previously Unrecognized 22q13.2 Microdeletion Syndrome That Encompasses TCF20 and TNFRSF13C." *American Journal of Medical Genetics. Part A* 176, no. 12: 2791–2797.

Verpelli, C., E. Dvoretskova, C. Vicidomini, et al. 2011. "Importance of Shank3 Protein in Regulating Metabotropic Glutamate Receptor 5 (mGluR5) Expression and Signaling at Synapses." *Journal of Biological Chemistry* 286, no. 40: 34839–34850.

Verpelli, C., G. Piccoli, A. Zanchi, et al. 2010. "Synaptic Activity Controls Dendritic Spine Morphology by Modulating eEF2-Dependent BDNF Synthesis." *Journal of Neuroscience* 30, no. 17: 5830–5842.

Verpelli, C., and C. Sala. 2012. "Molecular and Synaptic Defects in Intellectual Disability Syndromes." *Current Opinion in Neurobiology* 22, no. 3: 530–536.

Vetrini, F., S. McKee, J. A. Rosenfeld, et al. 2019. "De Novo and Inherited TCF20 Pathogenic Variants Are Associated With Intellectual Disability, Dysmorphic Features, Hypotonia, and Neurological Impairments With Similarities to Smith-Magenis Syndrome." *Genome Medicine* 11, no. 1: 12.

Vicidomini, C., L. Ponzoni, D. Lim, et al. 2017. "Pharmacological Enhancement of mGlu5 Receptors Rescues Behavioral Deficits in SHANK3 Knock-Out Mice." *Molecular Psychiatry* 22, no. 5: 689–702.

Walikonis, R., O. Jensen, M. Mann, D. J. Provance, J. Mercer, and M. Kennedy. 2000. "Identification of Proteins in the Postsynaptic Density Fraction by Mass Spectrometry." *Journal of Neuroscience* 20: 4069–4080.

Wiegreffe, C., S. Feldmann, S. Gaessler, and S. Britsch. 2017. "Time-Lapse Confocal Imaging of Migrating Neurons in Organotypic Slice Culture of Embryonic Mouse Brain Using in Utero Electroporation." *Journal of Visualized Experiments* 125: 55886.

Wiegreffe, C., R. Simon, K. Peschkes, et al. 2015. "Bcl11a (Ctip1) Controls Migration of Cortical Projection Neurons Through Regulation of Sema3c." *Neuron* 87, no. 2: 311–325.

Wiznerowicz, M., and D. Trono. 2003. "Conditional Suppression of Cellular Genes: Lentivirus Vector-Mediated Drug-Inducible RNA Interference." *Journal of Virology* 77, no. 16: 8957–8961.

Zhang, J., D. Zhang, J. S. McQuade, M. Behbehani, J. Z. Tsien, and M. Xu. 2002. "C-Fos Regulates Neuronal Excitability and Survival." *Nature Genetics* 30, no. 4: 416–420.

Zhou, J., H. Hamdan, H. K. Yalamanchili, et al. 2022. "Disruption of MeCP2-TCF20 Complex Underlies Distinct Neurodevelopmental Disorders." *Proceedings of the National Academy of Sciences of the United States of America* 119, no. 4: e2119078119.

Supporting Information

Additional supporting information can be found online in the Supporting Information section.